Deep Meteoric Water Circulation in Earth's Crust

Jennifer McIntosh[1,1,1] and Grant Ferguson[2,2,2]

[1]University of Arizona
[2]University of Saskatchewan

November 30, 2022

Abstract

Deep meteoric waters comprise a key component of the hydrologic cycle, transferring water, energy, and life between the earth's surface and deeper crustal environments, yet little is known about the nature and extent of meteoric water circulation. Using water stable isotopes, we show that maximum circulation depths of meteoric waters across North America vary considerably from <1 to 5 km, with the deepest circulation in western North America in areas of greater topographic relief. Shallower circulation occurs in sedimentary and shield-type environments with subdued topography. The amount of topographic relief available to drive regional groundwater flow and flush saline fluids is an important control on the extent of meteoric water circulation, in addition to permeability. The presence of an active flow system in the upper few kilometers of the Earth's crust and stagnant brines trapped by negative buoyancy offers a new framework for understanding deep groundwater systems.

Deep Meteoric Water Circulation in Earth's Crust

Jennifer C. McIntosh[1,2,*,†] and Grant Ferguson[1,2,†]

1. Hydrology and Atmospheric Sciences, University of Arizona, Tucson, AZ 85721 USA
2. Civil, Geological and Environmental Engineering, University of Saskatchewan, Saskatoon, SK CA

**corresponding author: jenmc@email.arizona.edu; 520-626-2282*

†These authors contributed equally to this work.

Key Points

- Maximum circulation depths of meteoric waters vary considerably from <1 to 5km across North America
- The deepest meteoric water circulation occurs in mountainous terrains in western North America
- Topographic gradients and fluid density are important controls on the extent of meteoric water circulation

Abstract

Deep meteoric waters comprise a key component of the hydrologic cycle, transferring water, energy, and life between the earth's surface and deeper crustal environments, yet little is known about the nature and extent of meteoric water circulation. Using water stable isotopes, we show that maximum circulation depths of meteoric waters across North America vary considerably from <1 to 5 km, with the deepest circulation in western North America in areas of greater topographic relief. Shallower circulation occurs in sedimentary and shield-type environments with subdued topography. The amount of topographic relief available to drive regional groundwater flow and flush saline fluids is an important control on the extent of meteoric water circulation, in addition to permeability. The presence of an active flow system in the upper few kilometers of the Earth's crust and stagnant brines trapped by negative buoyancy offers a new framework for understanding deep groundwater systems.

Plain Language Summary

Deep circulation of waters, coming from precipitation, connects the Earth's surface with deeper subsurface environments, transferring water, energy and life critical for key processes, such as deep mineral weathering and release of nutrients, and geothermal energy systems. Deeper, more saline groundwater is typically only weakly connected to the rest of the hydrologic cycle. The penetration depth of precipitation-derived waters and the bottom of the more active hydrologic cycle is relatively unknown. This study shows the depth of meteoric water circulation varies considerably across North America as a function of topography and fluid density, in

addition to permeability. Study results help constrain locations of deeper meteoric water penetration and potential hydrologic connections to the earth’s surface, which has important implications for the extent of water resources and transport and long-term storage of anthropogenic contaminants in the subsurface.

Index Terms and Keywords

1829-Groundwater hydrology

1041 - Stable isotope geochemistry

1832-Groundwater transport

1402-Critical Zone

1. Introduction

The extent and controls on deep groundwater circulation are poorly understood, creating challenges for groundwater resource assessment (Gleeson et al., 2016; Richey et al., 2015), waste isolation (Cherry et al., 2014; Ferguson, McIntosh, Perrone, et al., 2018), integration of groundwater into catchment hydrology (Condon et al., 2020; Frisbee et al., 2017) and Critical Zone science (Küsel et al., 2016), and the distribution and evolution of life in the subsurface (Lollar et al., 2019; Warr et al., 2018). Permeability exerts an important control on the rate of groundwater circulation (and groundwater age) and there have been a number of attempts to assess the variations in permeability with depth (Achtziger-Zupančič et al., 2017; Ingebritsen & Manning, 1999; Stober & Bucher, 2007). Permeability generally decreases with depth and residence times increase, however there is no conclusive evidence that groundwater circulation would cease due to the low permeabilities found at depth (Ingebritsen et al., 2006).

There have been comparatively few studies that have examined the extent of meteoric groundwater circulation through compiling geochemical and isotopic evidence. An examination of the origin of waters in sedimentary basins in North America suggested that topography and fluid density control the extent of meteoric water circulation rather than permeability (Ferguson, McIntosh, Grasby, et al., 2018). That study demonstrated that there is insufficient topography to flush dense brines from the deepest extents of many basins, despite sufficient permeability. These results were in agreement with δ^2H and δ^{18}O values that fell beneath the GMWL or a range of other geochemical measures, such as low Cl:Br ratios, that indicated that there was residual paleo-evaporated seawater present in the basin. Here, we build on those findings to assess the depth to which flushing by meteoric water would be possible in different geologic terrains at the continental scale using water stable isotopes (δ^2H and $\delta^{18}O$). We show that the maximum circulation depth varies considerably over a range of geological environments across North America and this appears to be associated with the amount of topographic relief available to overcome the negative buoyancy associated with the density of saline fluids at depth.

2. Distribution of Meteoric Waters

Meteoric waters typically have δ^2H and $\delta^{18}O$ values that fall near the global meteoric water line (GMWL) (Craig, 1961), and this can be used to delineate groundwaters that originate as precipitation and have not been significantly modified by water-rock reactions or mixing with non-meteoric fluids (Ferguson, McIntosh, Grasby, et al., 2018) (Figure 1a). Non-meteoric waters that deviate from the GMWL can be identified in terms of deuterium excess (D excess) relative to the GMWL (Dansgaard, 1964):

$$D\ excess\ = \delta^2 H - \ 8\ x\ \delta^{18} O \qquad [1]$$

Recognizing that shifts away from the GMWL can occur due to changes in $\delta^{18}O$, this can also be expressed as oxygen depletion (^{18}O depletion) (Kloppmann et al., 2002):

$$^{18}O\ depletion\ = {\delta^2 H}/{8} - \ \delta^{18}O \quad [2]$$

At the local scale, meteoric waters plot along local meteoric water lines that have slightly different slopes and intercepts from the GMWL, depending on local climatic conditions. These local deviations may over- or underestimate the D excess and ^{18}O depletion (Kloppmann et al, 2002), and alter the maximum circulation depths approximated in this study.

Deeper groundwaters that originated as evaporated seawater (e.g., sedimentary basin brines) typically have δ^2H and $\delta^{18}O$ values that plot beneath the GMWL (i.e. negative D excess and negative ^{18}O depletion values) (Kharaka & Hanor, 2003). High-temperature (geothermal) waters plot to the right of the GMWL, enriched in ^{18}O from high temperature isotope exchange with minerals; also displaying negative apparent D excess values (Truesdell & Hulston, 1980). Deep saline waters in cratonic (shield-type) environments often plot to the left of or above the GMWL due to low temperature water-rock interactions at low water to rock ratios that have modified either seawater, hydrothermal fluids, and/or meteoric water over long time periods (Fritz & Frape, 1982; Warr et al., 2020). Fluids that have interacted with CO_2 can also plot to the left of the GMWL or to the right (Karolytė et al., 2017).

Here we examine δ^2H and $\delta^{18}O$ data from water and energy wells and mine inflows to determine the maximum depth of meteoric water circulation. We supplement these data with estimated circulation depths for thermal springs where δ^2H and $\delta^{18}O$ values of discharged waters fall along the GMWL.

3. Methods

3.1. Databases and Mapping

The primary databases used to compile δ^2H and $\delta^{18}O$ data from wells for this study were the USGS Produced Waters database (Blondes et al., 2016) and data compiled for the Canadian Shield (Stotler et al., 2012). These data were supplemented by data from additional studies (Clark et al., 1998; Mariner & Janik, 1995; McIntosh et al., 2002, 2008, 2010; Osburn et al., 2019; Zhang et al., 2009). These datasets were culled to consider only those samples that provided a well location and depth. Additional data from the USGS NAWQA dataset (USGS, 2020) were also used to understand the distribution of meteoric water with depth in this study, but were not considered during mapping because of the shallow depth of most water supply wells and associated groundwater quality monitoring.

3.2. Estimating Meteoric Water Circulation Depths

Meteoric waters are typically defined as waters with δ^2H and $\delta^{18}O$ values falling near the GMWL. However, meteoric waters vary in their distance from the meteoric water line due to a range of processes, such as partial evaporation and convective air mass mixing that create local meteoric water lines (Jasechko, 2019). Tolerances for where meteoric waters fall around the GMWL are not typically defined quantitatively. Here, we consider waters with D excess values falling between -10 and 30‰ (20‰ variability in δ^2H or 2.5‰ variability in $\delta^{18}O$ around the GMWL) as meteoric waters.

To supplement δ^2H and $\delta^{18}O$ data from wells, we used studies that have estimated maximum temperatures from aqueous geothermometry on samples collected from thermal springs discharging meteoric water (Davisson et al., 1994; Frisbee et al., 2017; Grasby et al., 2016; Grasby & Hutcheon, 2001; Mayo & Loucks, 1995; Pepin et al., 2015). Those studies used local geothermal gradients to estimate the circulation depth required to obtain those maximum temperatures.

The maximum depth of circulation was estimated by determining the maximum depth of water samples with a D excess value falling between -10 and 30‰ or estimated circulation depth of a thermal spring with a meteoric water isotope signature based on a 2 degree by 2 degree grid across North America. Over much of North America, especially outside of oil and gas producing regions, the availability of deep samples is limited, and our mapped results are likely to underestimate the depth to which meteoric water is present. In addition, the approach used here underestimates meteoric water circulation depth by not considering deeper meteoric waters that have been isotopically-altered through low or high temperature water-rock reactions, or through isotopic exchange with CO_2. Where no samples deeper than 500 m were available, the grid spaces were left blank during mapping.

3.3. Assessment of Topography and Driving Force Ratio

We assess the possibility that the distribution of meteoric waters is controlled by the amount of topography available to drive regional groundwater flow and the negative buoyancy of dense, saline fluids at depth. Darcy's law for variable density groundwater flow can be written as:

$$q = \frac{-\mu}{\mu_o} K \left(\nabla h_o - \frac{\Delta\rho}{\rho_o} \nabla \mathrm{z} \right) \qquad [3]$$

Where q is specific discharge, μ is viscosity, μ_o is a reference viscosity, h_o is hydraulic head at a given reference density, ρ is density, ρ_o is reference density (commonly assumed to be 1,000 kg/m^3) and z is elevation head (Figure 2).

And

$$h_o = \frac{p}{\rho_o g} + z \qquad [4]$$

Where p is fluid pressure and g is acceleration due to gravity. The force driving groundwater flow, which determines the magnitude and direction of the hydraulic gradient, can be described as (Bachu, 1995):

$$F = -\frac{g\rho_o}{\rho} \left(\nabla h_o + \frac{\nabla\rho}{\rho_o} \nabla E \right) = F_p + F_b \qquad [5]$$

Where ∇h_o is the hydraulic gradient based on a reference density and ∇E is the average structural gradient of the groundwater flow system (i.e. the slope that the water must travel along to exit the groundwater system). The relative importance *of* F_p, which is the force associated with topographic differences, and F_b , which is the force of negative buoyancy, is described by the driving force ratio (*DFR*), which is defined as follows (Bachu, 1995):

$$DFR = \left(\frac{\Delta\rho}{\rho_o} \frac{|\nabla E|}{|\nabla h|_o} \right) \qquad [6]$$

This approach was originally intended to assess errors arising from using potentiometric maps based on reference densities, but has been extended to examine where dense brines would be trapped by negative buoyancy in sedimentary basins (Ferguson, McIntosh, Grasby, et al., 2018). In this case, the condition necessary for waters to stagnate can be described as:

$$\nabla h_o = \frac{\Delta\rho}{\rho_o}\nabla E \qquad [7]$$

For systems where the water table closely follows the topography and the highest hydraulic head in the flow system overlies the deepest point of the flow system, [3] can be approximated as:

$$\Delta h_{max} = \frac{\rho-\rho_o}{\rho_o} z_{max} \qquad [8]$$

Where Δh_{max} is the maximum hydraulic head and z_{max} is the maximum circulation depth. Where h_o is insufficient to overcome the density contrast, dense waters below z_{max} are isolated from the overlying topographically-driven flow system and will not discharge to surface water bodies. The case where the deepest part of the flow system coincides with the maximum ground surface elevation will underestimate *DFR* in most cases. If the deepest part of the flow system coincides with its horizontal midpoint, $|\nabla E|$ would increase by a factor of two and [5] would overestimate circulation depth by the same factor.

Here, we use topographic drops as a proxy for the maximum hydraulic head change. This will tend to overestimate hydraulic gradients, especially in areas with higher permeability, lower recharge rates or higher topography (Gleeson et al., 2011), resulting in overestimation of the maximum circulation depth. Maximum topographic drops were calculated from the USGS GTOPO30 digital elevation model (USGS, 1997) on a 2 degree x 2 degree grid across North America using QGIS. We chose a gridded approach because there are many areas of North America where there are no obvious boundaries for deep groundwater flow systems. Permeability contrasts associated with geological contacts have been used to constrain these in some studies (Ferguson, McIntosh, Grasby, et al., 2018; Condon et al., 2020). This approach is ill-suited for the current problem because it assumes that meteoric water will not circulate through lower permeability rocks. Watershed-based approaches are also problematic because deep groundwater flow often transfers water between watersheds (Fan, 2019). These topographic drops are then compared to the sample depths in each grid block to calculate the topographic drop to depth ratio.

4. Maximum Circulation Depth

The maximum circulation depth of meteoric waters in North America ranges from less than 1 km in eastern North America to approximately 5 km in the west (Figure 3). Deeper circulation depths occur in areas of greater topographic relief and the greatest circulation depths are associated with thermal springs. The shallowest circulation depths are associated with oil/gas produced waters in sedimentary basins and mines in crystalline bedrock.

Lithology does not appear to exert a strong control on circulation depth. The circulation depths in the Canadian Shield are similar to many sedimentary basins in midcontinent North America, despite the large differences in permeability (Figure 1b). The extent of meteoric water circulation in the Canadian Shield roughly coincides with the depth where bulk permeability approaches the matrix permeability at ~1 km (Achtziger-Zupančič et al., 2017). While permeability and meteoric water circulation appear to coincide in the Canadian Shield, examination of other environments suggests that permeability might not be the only controlling factor.

In sedimentary basins, decreases in permeability with depth do not explain the extent of meteoric water circulation. Over much of central North America, circulation depths are less than 2 km. Relatively high permeability (>10^{-16} m^2) sandstone and carbonate aquifers are present at the bottom of many sedimentary basins (> 2 km depth) (Figure 1b). Yet these basal aquifer systems often contain non-meteoric waters, derived from paleo-evaporated seawater (Bein & Dutton, 1993; Ferguson et al., 2007; Stueber & Walter, 1991). Conventional oil and gas production and saltwater disposal are common in these deep strata (Ferguson, 2015; Scanlon et al., 2019; Zhang et al., 2016), indicating that appreciable groundwater flow rates are possible where hydraulic gradients are sufficiently high. In some cases, such as the lower Paleozoic aquifers of the Williston Basin, these systems appear to be hydraulically continuous between known recharge and discharge areas (Bachu and Hitchon, 1996; Grasby et al., 2000; Ferguson et al., 2007). We hypothesize an additional mechanism for trapping saline fluids at depth in sedimentary and crystalline environments - due to negative buoyancy.

The deepest circulation of meteoric groundwater is found in thermal springs in mountainous areas of western North America. The median circulation depth of the 38 springs compiled here was 2.6 km and this approach is thought to underestimate circulation depth due to geochemical re-equilibration of waters as they interact with the rock mass as they rise toward the discharge area, and due to mixing of waters from different depths (Ferguson et al., 2009). The results presented here are similar to those found in the Alps (Diamond et al., 2018; Luijendijk et al., 2020). Very little is known about the permeability distribution of these systems from direct measurements, but numerical modelling indicates that country rock values on the order of 10^{-16} m^2 are required to supply a sufficient amount of water to a fault to support the formation of thermal springs (Forster & Smith, 1989).

The link between topography and circulation depth indicates that the forces driving circulation may exert a substantial control on how deep meteoric water penetrates into the Earth's crust. Deep groundwaters that do not fall on the GMWL typically have salinities that are several times that of seawater (Fritz & Frape, 1982; Kharaka & Hanor, 2003). These highly saline waters appear to be ubiquitous at depth in both sedimentary environments (Kharaka & Hanor, 2003) and in crystalline bedrock (Stotler et al., 2012; Warr et al., 2018) and are also thought to be present in the lower crust (Manning, 2018). Due to their high salinities (TDS~300 g/L), these waters have densities that approach 1,200 kg/m^3 (Adams & Bachu, 2002). For regional groundwater flow systems where the water table coincides with the ground surface, the topographic drop to depth ratio must exceed 0.2 for a 1,200 kg/m^3 density brine to allow for it to be flushed by meteoric water (Equation 8). Actual topographic drop to depth ratios required for flushing would be greater than 0.2, as regional hydraulic gradients are less than topographic gradients.

Meteoric waters with D excess values between -10 and 30‰ and ^{18}O depletion values from -1.25 to 3.75‰, corresponding to the GMWL, tend to have large topographic drops relative to their depths. Where topographic drop to depth ratios of less than 0.2 and trapping due to negative buoyancy is expected, D excess values tend to be less than -10‰ and ^{18}O depletion values tend to be less than -1.25‰ (Figure 4). In some cases, meteoric waters are found at topographic drop to depth ratios of less than 0.2, in locations where increased hydraulic gradients from Pleistocene ice sheets (McIntosh et al., 2002; McIntosh et al., 2011) or due to sea-level low stands in coastal aquifers (Person et al., 2003; Cohen et al., 2010; Post et al., 2013) enhanced meteoric circulation and flushing of basinal brines or seawater, respectively.

The most negative D excess and ^{18}O depletion values (i.e., most saline basin brines) are associated with topographic drop to depth ratios less than ~1, although a variety of D excess and ^{18}O depletion values are found at these ratios. ^{18}O depletion and apparent D excess values exceeding +3.75‰ and +30‰, respectively (i.e., shield-type brines) tend to be associated with topographic drop to depth ratios of ~1.

Many of the samples with D excess and ^{18}O depletion values outside of the range expected from meteoric waters have topographic drop to depth ratios greater than the critical value (0.2) or higher than is required to displace a brine with a density of 1,200 kg/m^3 (Figure 4). Many of these samples likely have a component of meteoric water that is actively circulating or are residual brines that are still in the process of being flushed by regional groundwater flow, which may take millions of years or more due to the presence of low permeability units. Ingebritsen and Manning (1999) estimate that crustal permeability is typically greater than 10^{-16} m^{12} in the upper 5,000 m, which would allow for movement of fluids over distances of kilometers over periods of a few million years. In extreme cases, such as permeabilities below 10^{-20} m^2 known to exist in intact crystalline rock (Achtziger-Zupančič et al., 2017), evaporites (Bredehoeft, 1988), and shale (Neuzil, 1986), advective transport of only a few m in 100s of millions of years is possible, preventing any meaningful flushing by meteoric waters. For example, the most ancient shield-type brines may be trapped in isolated fractures that are disconnected from active circulation systems due to extremely low permeabilities (Warr et al., 2018).

Other non-meteoric water samples that have a topographic drop to depth ratio greater than the critical value (0.2) could be trapped by negative buoyancy due to the overestimation of the hydraulic gradient by using topography as a proxy (e.g., in areas with deep water tables that are a subdued reflection of surface topography) or by underestimating the structural gradient (e.g., instances where the highest hydraulic head values does not overlie the maximum circulation depth) (Ferguson, McIntosh, Grasby, et al., 2018).

5. Conclusions - Rethinking the Extent of the Deep Hydrological Cycle

Many previous studies have assumed that groundwater resources extended to 1 or 2 km globally (Gleeson et al., 2016; Nace, 1969; Richey et al., 2015). The remarkable spatial variability of circulation depth suggests that previous estimates of the volume (Gleeson et al., 2016; Nace, 1969; Richey et al., 2015) and residence times of groundwater at global scales (Befus et al., 2017) are less certain, depending on topographic gradients, permeability structure and salinity distribution. Taking into account this variability and fluid drivers provides an opportunity to refine global estimates of groundwater volumes and circulation depths.

Topography and variations of fluid density with depth exert a strong control on the extent of the meteoric water circulation in the crust, in addition to permeability decreases, which have received more attention to-date as a primary constraint on the circulation of groundwater at depth (Achtziger-Zupančič et al.,2017; Ingebriten & Manning, 1999; Ingebritsen & Gleeson, 2017; Ranjram et al., 2015; Stober & Bucher, 2007). Global assessments of bulk permeability have suggested that groundwater flow is possible over most of the brittle crust, which extends to a depth of ~10 km (Ingebritsen & Manning, 1999). Our results indicate that circulation of meteoric water outside of orogenic belts is largely restricted to the upper 1 to 2 km, regardless of permeability and is influenced by topography and negative buoyancy. The inability of meteoric water to circulate to depths exceeding more than ~1 to 2 km over large areas of continents is consistent with observations of very old, saline waters at these depths in both cratons (Holland et al., 2013; Lippmann et al., 2003; Warr et al., 2018) and sedimentary basins (Castro et al., 1998; Zhou & Ballentine, 2006). It is also consistent with penetration depths of meteoric waters that have recently been in contact with the atmosphere based on the presence of tritium (Gleeson et al., 2016) and radiocarbon (Jasechko et al., 2017).

These results showing the importance of topographic gradients and fluid density elicit a change in how we characterize hydrogeologic systems. We have few tools other than sampling deep wells, boreholes or mines to characterize groundwater salinity and residence times at depth. In particular, deep wells are uncommon in mountainous regions (Markovich et al., 2019) – areas with the deepest meteoric water circulation – and beyond ~1 km in crystalline shield-type environments. The need for geophysical or other techniques to address the extent of meteoric groundwater in the Earth's crust represents a major challenge for the geosciences.

Acknowledgements

This project was supported by a Global Water Futures grant to Ferguson and McIntosh and an NSERC Discovery Grant to Ferguson. McIntosh also acknowledges funding from the W.M. Keck Foundation and CIFAR Earth4D: Subsurface Science and Exploration Program. Thank you to the reviewers for providing helpful comments that improved the manuscript. Data is available from Blondes et al. (2016), Clark et al. (1998), Davisson et al. (1994), Frisbee et al. (2017), Grasby et al. (2016), Grasby & Hutcheon (2001), Mayo & Loucks (1995), Mariner & Janik (1995), McIntosh et al. (2002; 2008; 2010), Osburn et al. (2019), Pepin et al. (2015), Stotler et al. (2012), USGS (2020), and Zhang et al. (2009).

References

Achtziger-Zupančič, P., Loew, S., & Mariethoz, G. (2017). A new global database to improve predictions of permeability distribution in crystalline rocks at site scale. *Journal of Geophysical Research: Solid Earth*, *122*(5), 3513–3539.

Adams, J., & Bachu, S. (2002). Equations of state for basin geofluids: algorithm review and intercomparison for brines. *Geofluids*, *2*(4), 257–271.

Bachu, S. (1995). Flow of variable-density formation water in deep sloping aquifers: review of methods of representation with case studies. *Journal of Hydrology*, *164*(1), 19–38.

Bachu, S., & Hitchon, B. (1996). Regional-scale flow of formation waters in the Williston Basin. *AAPG Bulletin, 80*(2), 248-264.

Befus, K. M., Jasechko, S., Luijendijk, E., Gleeson, T., & Cardenas, M. B. (2017). The rapid yet uneven turnover of Earth's groundwater. *Geophysical Research Letters, 44*(11), 5511-5520.

Bein, A., & Dutton, A. R. (1993). Origin, distribution, and movement of brine in the Permian Basin (USA): A model for displacement of connate brine. *Geological Society of America Bulletin*, *105*(6), 695–707.

Blondes, M. S., Gans, K. D., Thordsen, J. J., Reidy, M. E., Thomas, B., Engle, M. A., et al. (2016). US Geological Survey National Produced Waters Geochemical Database v2. 3 (PROVISIONAL). *United States Geological Survey*.

Bredehoeft, J. D. (1988). Will salt repositories be dry? *EOS, Transactions American Geophysical Union, 69*(9), 121-131.

Castro, M. C., Jambon, A., De Marsily, G., & Schlosser, P. (1998). Noble gases as natural tracers of water circulation in the Paris Basin: 1. Measurements and discussion of their origin and mechanisms of vertical transport in the basin. *Water Resources Research*, *34*(10), 2443–2466.

Cherry, J. A., Alley, W. M., & Parker, B. L. (2014). Geologic Disposal of Spent Nuclear Fuel. *The Bridge on Emerging Issues in Earth Resources Engineering*, *44*(1), 51–59.

Clark, J. F., Davisson, M. L., Hudson, G. B., & Macfarlane, P. A. (1998). Noble gases, stable isotopes, and radiocarbon as tracers of flow in the Dakota aquifer, Colorado and Kansas. *Journal of Hydrology*, *211*(1–4), 151–167.

Cohen, D., Person, M., Wang, P., Gable, C. W., Hutchinson, D., Marksamer, A., Dugan, B., Kooi, H., Groen, K., Lizarralde, D. & Evans, R. L. (2010). Origin and extent of fresh paleowaters on the Atlantic continental shelf, USA. *Groundwater, 48*(1), 143-158.

Condon, L. E., Markovich, K. H., Kelleher, C. A., McDonnell, J. J., Ferguson, G., & McIntosh, J. C. (2020). Where is the bottom of a watershed? *Water Resources Research*, *56*(3).

Craig, H. (1961). Isotopic variations in meteoric waters. *Science*, *133*(3465), 1702–1703.

Dansgaard, W. (1964). Stable isotopes in precipitation. *Tellus*, *16*(4), 436–468.

Davisson, M. L., Presser, T. S., & Criss, R. E. (1994). Geochemistry of tectonically expelled fluids from the northern Coast ranges, Rumsey Hills, California, USA. *Geochimica et Cosmochimica Acta*, *58*(7), 1687–1699.

Diamond, L. W., Wanner, C., & Waber, H. N. (2018). Penetration depth of meteoric water in orogenic geothermal systems. *Geology*, *46*(12), 1063–1066.

Fan, Y. (2019). Are catchments leaky? *Wiley Interdisciplinary Reviews: Water*, *6*(6), e1386.

Ferguson, G. (2015). Deep Injection of Waste Water in the Western Canada Sedimentary Basin. *Groundwater*, *53*(2), 187–194. https://doi.org/10.1111/gwat.12198

Ferguson, G., Betcher, R. N., & Grasby, S. E. (2007). Hydrogeology of the Winnipeg Formation in Manitoba, Canada. *Hydrogeology Journal*, *15*(3), 573–587. https://doi.org/10.1007/s10040-006-0130-4

Ferguson, G., Grasby, S. E., & Hindle, S. R. (2009). What do aqueous geothermometers really tell us? *Geofluids*, *9*(1), 39–48. https://doi.org/10.1111/j.1468-8123.2008.00237.x

Ferguson, G., McIntosh, J. C., Perrone, D., & Jasechko, S. (2018). Competition for shrinking window of low salinity groundwater. *Environmental Research Letters*, *13*, 114013.

Ferguson, G., McIntosh, J. C., Grasby, S. E., Hendry, M. J., Jasechko, S., Lindsay, M. B. J., & Luijendijk, E. (2018). The Persistence of Brines in Sedimentary Basins. *Geophysical Research Letters*, *45*(10), 4851–4858.

Forster, C., & Smith, L. (1989). The influence of groundwater flow on thermal regimes in mountainous terrain: A model study. *Journal of Geophysical Research: Solid Earth*, *94*(B7), 9439–9451. https://doi.org/10.1029/JB094iB07p09439

Frisbee, M. D., Tolley, D. G., & Wilson, J. L. (2017). Field estimates of groundwater circulation depths in two mountainous watersheds in the western US and the effect of deep circulation on solute concentrations in streamflow. *Water Resources Research*, *53*(4), 2693–2715.

Fritz, P., & Frape, S. t. (1982). Saline groundwaters in the Canadian Shield—a first overview. *Chemical Geology*, *36*(1), 179–190.

Gleeson, T., Marklund, L., Smith, L., & Manning, A. H. (2011). Classifying the water table at regional to continental scales. *Geophysical Research Letters*, *38*(5).

Gleeson, T., Befus, K. M., Jasechko, S., Luijendijk, E., & Cardenas, M. B. (2016). The global volume and distribution of modern groundwater. *Nature Geoscience*, *9*(2), 161–167.

Grasby, S. E., & Hutcheon, I. (2001). Controls on the distribution of thermal springs in the southern Canadian Cordillera. *Canadian Journal of Earth Sciences*, *38*(3), 427–440.

Grasby, S. E., Ferguson, G., Brady, A., Sharp, C., Dunfield, P., & McMechan, M. (2016). Deep groundwater circulation and associated methane leakage in the northern Canadian Rocky Mountains. *Applied Geochemistry*, *68*, 10–18.

Grasby, S., Osadetz, K., Betcher, R., & Render, F. (2000). Reversal of the regional-scale flow system of the Williston basin in response to Pleistocene glaciation. *Geology, 28*(7), 635-638.

Holland, G., Lollar, B. S., Li, L., Lacrampe-Couloume, G., Slater, G., & Ballentine, C. (2013). Deep fracture fluids isolated in the crust since the Precambrian era. *Nature*, *497*(7449), 357.

Ingebritsen, S. E., & Gleeson, T. (2017). Crustal permeability. *Hydrogeology Journal*, *25*(8), 2221–2224.

Ingebritsen, S. E., & Manning, C. E. (1999). Geological implications of a permeability-depth curve for the continental crust. *Geology*, *27*(12), 1107–1110.

Ingebritsen, S. E., Sanford, W. E., & Neuzil, C. (2006). *Groundwater in Geologic Processes*. Cambridge University Press.

Jasechko, S. (2019). Global isotope hydrogeology—Review. *Reviews of Geophysics*, *57*(3), 835–965.

Jasechko, S., Perrone, D., Befus, K. M., Cardenas, M. B., Ferguson, G., Gleeson, T., et al. (2017). Global aquifers dominated by fossil groundwaters but wells vulnerable to modern contamination. *Nature Geoscience*, *10*(6), 425–429.

Karolytė, R., Serno, S., Johnson, G., & Gilfillan, S. M. (2017). The influence of oxygen isotope exchange between CO_2 and H_2O in natural CO_2-rich spring waters: Implications for geothermometry. *Applied Geochemistry*, *84*, 173–186.

Kharaka, Y. K., & Hanor, J. S. (2003). Deep fluids in the continents: I. Sedimentary basins. *Treatise on Geochemistry*, *5*, 605.

Kloppmann, W., Girard, J.-P., & Négrel, P. (2002). Exotic stable isotope compositions of saline waters and brines from the crystalline basement. *Chemical Geology*, *184*(1–2), 49–70.

Küsel, K., Totsche, K. U., Trumbore, S. E., Lehmann, R., Steinhäuser, C., & Herrmann, M. (2016). How deep can surface signals be traced in the critical zone? Merging biodiversity with biogeochemistry research in a central German Muschelkalk landscape. *Frontiers in Earth Science*, *4*, 32.

Lippmann, J., Stute, M., Torgersen, T., Moser, D. P., Hall, J. A., Lin, L., et al. (2003). Dating ultra-deep mine waters with noble gases and 36Cl, Witwatersrand Basin, South Africa. *Geochimica et Cosmochimica Acta*, *67*(23), 4597–4619.

Lollar, G. S., Warr, O., Telling, J., Osburn, M. R., & Lollar, B. S. (2019). ‘Follow the Water’: Hydrogeochemical Constraints on Microbial Investigations 2.4 km Below Surface at the Kidd Creek Deep Fluid and Deep Life Observatory. *Geomicrobiology Journal*, 1–14.

Luijendijk, E., Winter, T., Köhler, S., Ferguson, G., von Hagke, C. & Scibek, J. (2020) Using thermal springs to quantify deep groundwater flow and its thermal footprint in the Alps and a comparison with North American orogens. *Geophysical Research Letters,* doi:10.1029/2020GL090134.

Manning, C. E. (2018). Fluids of the lower crust: deep is different. *Annual Review of Earth and Planetary Sciences*, *46*, 67–97.

Mariner, R. H., & Janik, C. J. (1995). *Geochemical data and conceptual model for the Steamboat Hills geothermal system, Washoe County, Nevada*. Geothermal Resources Council, Davis, CA (United States).

Markovich, K. H., Manning, A. H., Condon, L. E., & McIntosh, J. C. (2019). Mountain-Block Recharge: A Review of Current Understanding. *Water Resources Research*, *55*(11), 8278–8304.

Mayo, A. L., & Loucks, M. D. (1995). Solute and isotopic geochemistry and ground water flow in the central Wasatch Range, Utah. *Journal of Hydrology*, *172*(1–4), 31–59.

McIntosh, J. C., Walter, L., & Martini, A. (2002). Pleistocene recharge to midcontinent basins: effects on salinity structure and microbial gas generation. *Geochimica et Cosmochimica Acta*, *66*(10), 1681–1700.

McIntosh, J. C., Martini, A., Petsch, S., Huang, R., & Nüsslein, K. (2008). Biogeochemistry of the Forest City Basin coalbed methane play. *International Journal of Coal Geology*, *76*(1–2), 111–118.

McIntosh, J. C., Warwick, P. D., Martini, A. M., & Osborn, S. G. (2010). Coupled hydrology and biogeochemistry of Paleocene–Eocene coal beds, northern Gulf of Mexico. *Bulletin*, *122*(7–8), 1248–1264.

McIntosh, J. C., Garven, G. & Hanor, J. S. (2011). Impacts of Pleistocene glaciation on large-scale groundwater flow and salinity in the Michigan Basin. *Geofluids, 11*(1), 18-33.

Medina, C. R., Rupp, J. A., & Barnes, D. A. (2011). Effects of reduction in porosity and permeability with depth on storage capacity and injectivity in deep saline aquifers: A case study from the Mount Simon Sandstone aquifer. *International Journal of Greenhouse Gas Control*, *5*(1), 146–156.

Nace, R. L. (1969). World water inventory and control. In R. J. Chorley (Ed.), *Water, Earth, and Man* (pp. 31–42). London, U.K.: Methuen.

Neuzil, C. E. (1986). Groundwater flow in low-permeability environments. *Water Resources Research, 22*(8), 1163-1195.

Osburn, M. R., Kruger, B., Masterson, A., Casar, C., & Amend, J. (2019). Establishment of the Deep Mine Microbial Observatory (DeMMO), South Dakota, USA, a geochemically stable portal into the deep subsurface. *Frontiers in Earth Science*, *7*, 196.

Pepin, J., Person, M., Phillips, F., Kelley, S., Timmons, S., Owens, L., et al. (2015). Deep fluid circulation within crystalline basement rocks and the role of hydrologic windows in the formation of the Truth or Consequences, New Mexico low-temperature geothermal system. *Geofluids*, *15*(1–2), 139–160.

Person, M., Dugan, B., Swenson, J.B., Urbano, L., Stott, C., Taylor, J., & Willet, M. (2003). Pleistocene hydrogeology of the Atlantic continental shelf, New England. *Geological Society of America Bulletin, 115*(11), 1324-1343.

Phillips, D. (2019). *Reservoir Characterization and Modeling of Potash Mine Injection Wells in Saskatchewan*. University of Saskatchewan, Saskatoon, SK.

Post, V. E., Groen, J., Kooi, H., Person, M., Ge, S., & Edmunds, W. M. (2013). Offshore fresh groundwater reserves as a global phenomenon. *Nature, 504*(7478), 71-78.

Ranjram, M., Gleeson, T., & Luijendijk, E. (2015). Is the permeability of the crystalline rock in the shallow crust related to depth, lithology or tectonic setting? *Geofluids, 15*(1-2), 106-199.

Richey, A. S., Thomas, B. F., Lo, M., Famiglietti, J. S., Swenson, S., & Rodell, M. (2015). Uncertainty in global groundwater storage estimates in a Total Groundwater Stress framework. *Water Resources Research*, *51*(7), 5198–5216. https://doi.org/10.1002/2015WR017351

Scanlon, B. R., Weingarten, M. B., Murray, K. E., & Reedy, R. C. (2019). Managing Basin-Scale Fluid Budgets to Reduce Injection-Induced Seismicity from the Recent U.S. Shale Oil Revolution. *Seismological Research Letters*, *90*(1), 171–182. https://doi.org/10.1785/0220180223

Stober, I., & Bucher, K. (2007). Hydraulic properties of the crystalline basement. *Hydrogeology Journal*, *15*(2), 213–224.

Stotler, R., Frape, S., Ruskeeniemi, T., Pitkänen, P., & Blowes, D. (2012). The interglacial–glacial cycle and geochemical evolution of Canadian and Fennoscandian Shield groundwaters. *Geochimica et Cosmochimica Acta*, *76*, 45–67.

Stueber, A. M., & Walter, L. M. (1991). Origin and chemical evolution of formation waters from Silurian-Devonian strata in the Illinois Basin, USA. *Geochimica et Cosmochimica Acta*, *55*(1), 309–325.

Truesdell, A. H., & Hulston, J. R. (1980). Isotopic evidence on environments of geothermal systems. In Fritz, P., Fontes, J.Ch. (Eds.) *Handbook of environmental isotope geochemistry. Vol. 1,* Elsevier, Amsterdam, pp. 179-226.

USGS (1997). USGS 30 ARC-second Global Elevation Data, GTOPO30. Boulder, CO: Research Data Archive at the National Center for Atmospheric Research, Computational and Information Systems Laboratory. https://doi.org/10.5065/A1Z4-EE71

USGS (2020). National Water-Quality Assessment (NAWQA). Retrieved from https://www.usgs.gov/mission-areas/water-resources/science/national-water-quality-assessment-nawqa

Warr, O., Sherwood Lollar, B., Fellowes, J., Sutcliffe, C. N., McDermott, J. M., Holland, G., et al. (2018). Tracing ancient hydrogeological fracture network age and compartmentalisation using noble gases. *Geochimica et Cosmochimica Acta*, *222*, 340–362.

Warr, O., Giunta, T., Onstott, T., Kieft, T., Harris, R., Nisson, D., & Sherwood Lollar, B. (2020). Subsurface 18O Exchange at Low Temperatures: The (GMWL) Plot Thickens. Presented at the Goldschmidt Virtual 2020, The Geochemical Society.

Zhang, Y., Edel, S. S., Pepin, J., Person, M., Broadhead, R., Ortiz, J. P., et al. (2016). Exploring the potential linkages between oil-field brine reinjection, crystalline basement permeability, and triggered seismicity for the Dagger Draw Oil field, southeastern New Mexico, USA, using hydrologic modeling. *Geofluids*, *16*(5), 971–987.

Zhang, Y., Gable, C. W., Zyvoloski, G. A., & Walter, L. M. (2009). Hydrogeochemistry and gas compositions of the Uinta Basin: A regional-scale overview. *AAPG Bulletin*, *93*(8), 1087–1118.

Zhou, Z., & Ballentine, C. J. (2006). ^{4}He dating of groundwater associated with hydrocarbon reservoirs. *Chemical Geology*, *226*(3–4), 309–327.

Figure Captions:

Figure 1: Distribution of a) meteoric water and b) permeability with depth. Deuterium excess and ^{18}O depletion generally decreases with depth showing a transition from waters with a meteoric origin (D excess between -10 and 30‰ or ^{18}O depletion from -1.25 to 3.75‰, see inset for distribution along GMWL) to more negative values associated with paleo-evaporated seawater in sedimentary basins. Waters from several hundreds of m deep in the Canadian Shield tend to plot with more positive ^{18}O depletion (apparent negative D excess) values. Isotopic data references are included in the methods. Global databases of permeability (Achtziger-Zupančič et al., 2017; Ingebritsen & Manning, 1999) show permeability generally decreases with depth. Numerical models of thermal springs indicate elevated permeability is present to depths of several km in orogenic belts (Forster & Smith, 1989). However, similar permeabilities exist in regional aquifers in sedimentary basins (Medina et al., 2011; Phillips, 2019; Zhang et al., 2016) where non-meteoric waters are present.

Figure 2: Conceptual figure showing trade-off between topographic gradient and negative buoyancy from presence of dense brines in the Driving Force Ratio (DFR; Equation 6) controlling circulation depth of meteoric waters through a sedimentary basin and an underlying crystalline basement. h_o is hydraulic head at a given reference density, z_{max} is maximum circulation depth, F_p is the force associated with topographic differences, and F_b is the force of negative buoyancy.

Figure 3: Meteoric water circulation depth across North America. Depth of circulation as estimated from deepest sample with D excess value within 20‰ of the GMWL in a 2 degree by 2 degree grid. Squares with solid black outlines are produced waters, red outlines from estimates based on geothermometry from springs, and dashed outlines samples from mines or other projects in Precambrian rock. Isotopic data references are included in the methods.

Figure 4: Prediction of circulating vs stagnant fluids based on topographic gradients. D excess between -10 and 30‰ (^{18}O depletion from -1.25 to 3.75‰) values indicating meteoric waters mainly occur where topographic drop to depth ratios exceed 0.2, the theoretical critical value required for a brine with a density of 1,200 kg/m^3 to be trapped by negative buoyancy. Negative D excess indicative of non-meteoric, paleo-evaporated seawater derived brines tend to plot at low topographic drop to depth ratios. Strongly positive ^{18}O depletion (negative D excess) values found in shield environments tend to plot at topographic drop to depth ratios near the critical value for trapping by negative buoyancy.

Figure 1.

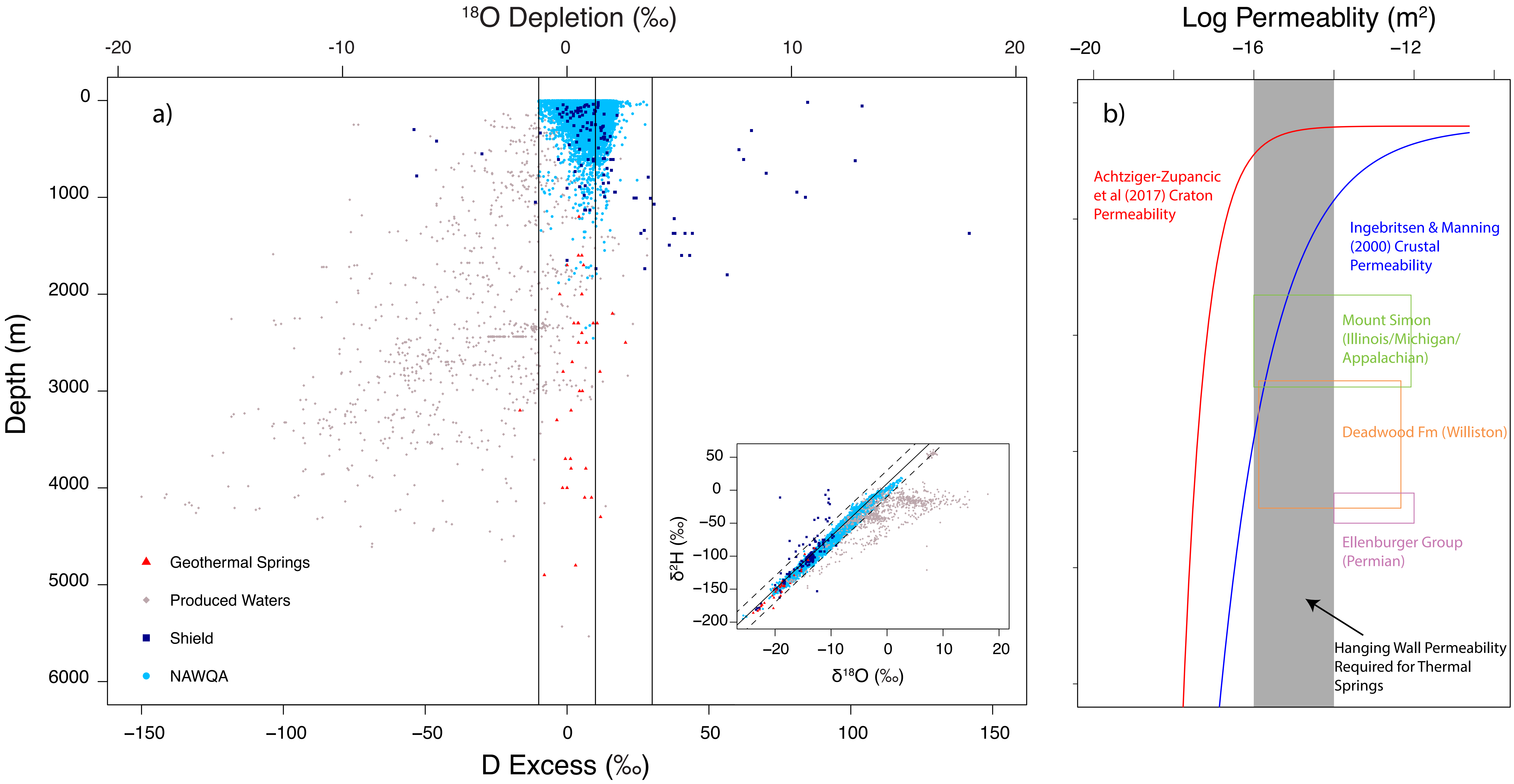

18O Depletion (‰)
a)
Depth (m)
D Excess (‰)
Geothermal Springs
Produced Waters
Shield
NAWQA
δ2H (‰)
δ18O (‰)
Log Permeablity (m2)
b)
Achtziger-Zupancic et al (2017) Craton Permeability
Ingebritsen & Manning (2000) Crustal Permeability
Mount Simon (Illinois/Michigan/ Appalachian)
Deadwood Fm (Williston)
Ellenburger Group (Permian)
Hanging Wall Permeability Required for Thermal Springs

Figure 2.

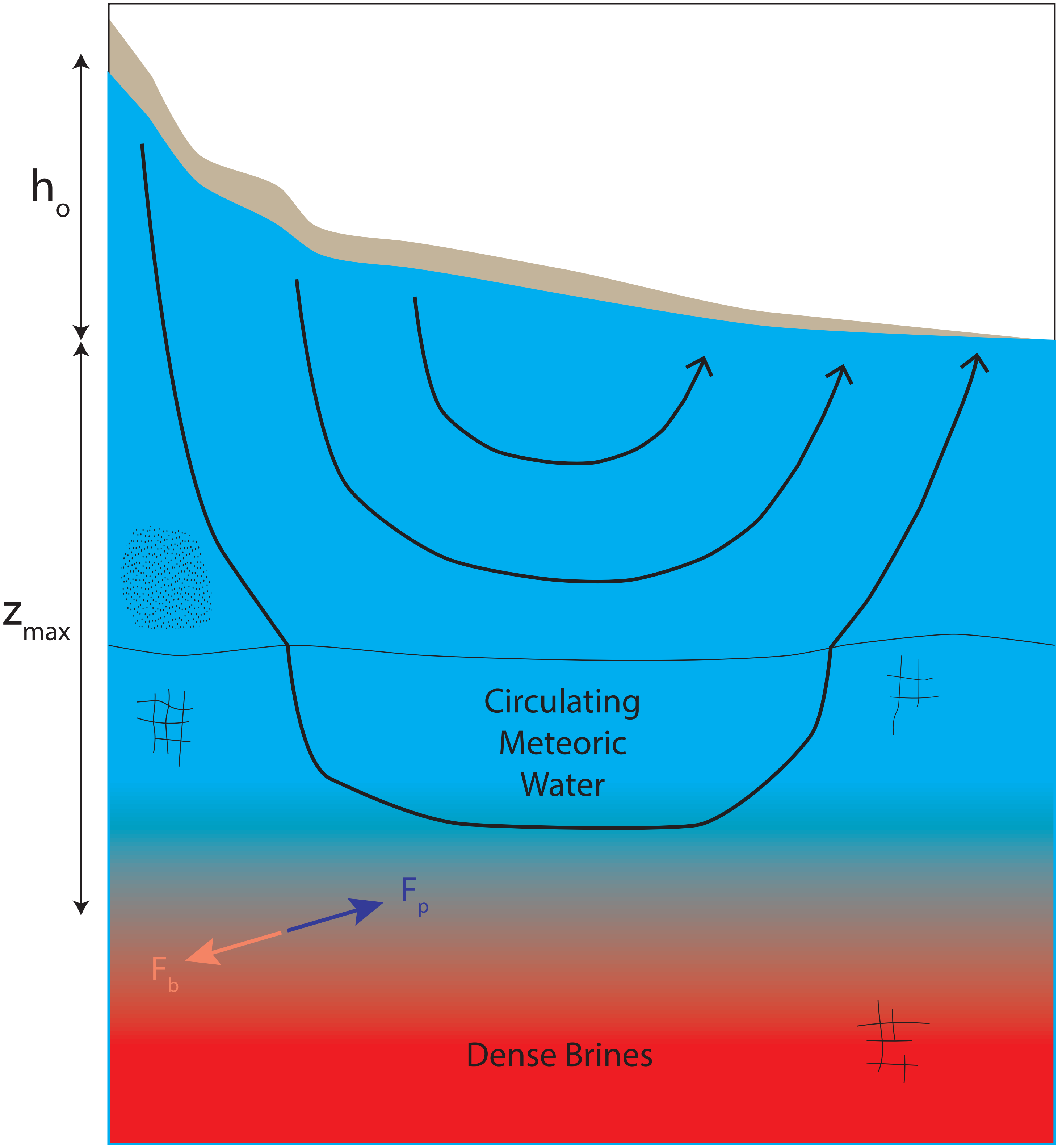

h_o
z_{max}
Circulating
Meteoric
Water
F_p
F_b
Dense Brines

Figure 3.

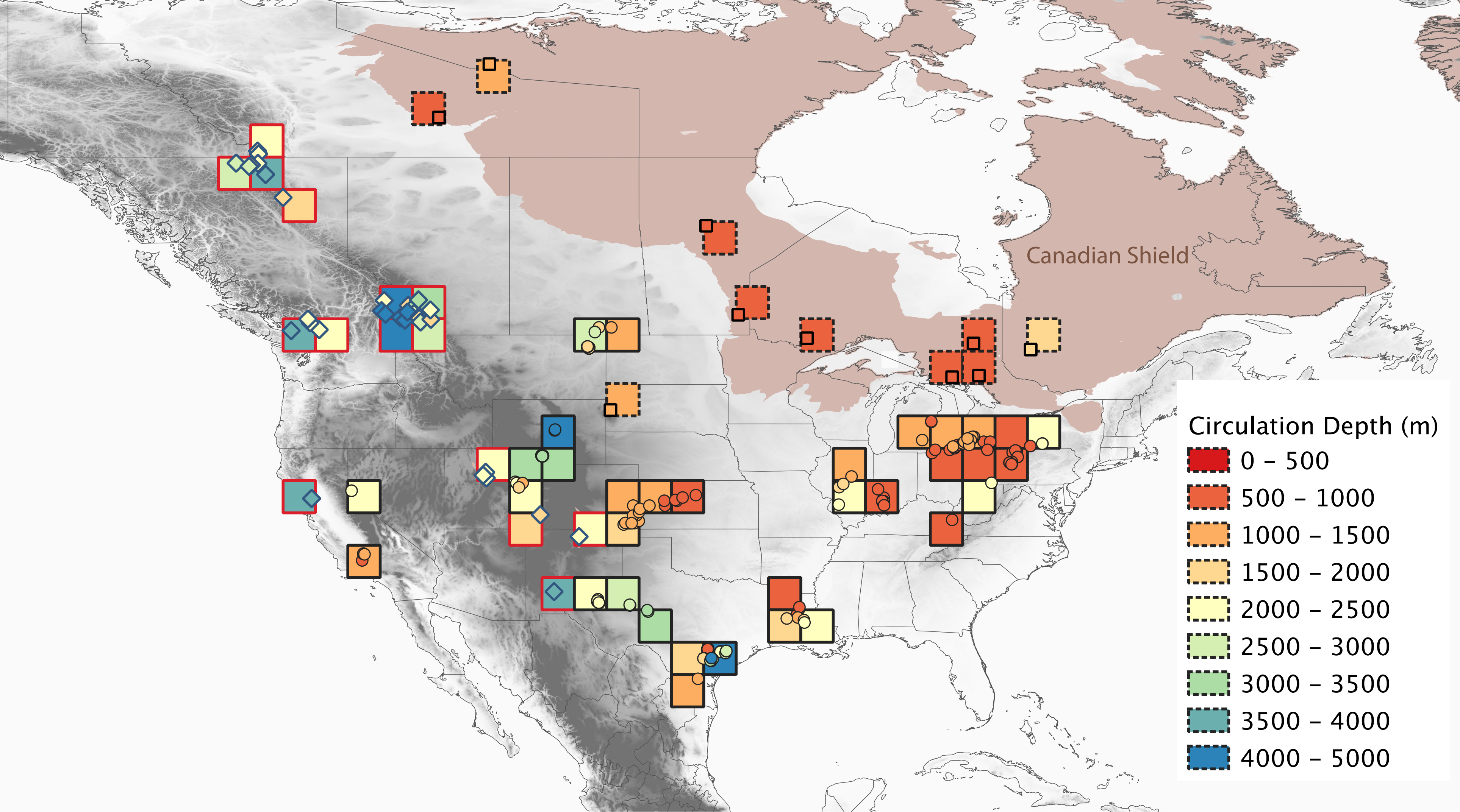
Canadian Shield
Circulation Depth (m)
0 – 500
500 – 1000
1000 – 1500
1500 – 2000
2000 – 2500
2500 – 3000
3000 – 3500
3500 – 4000
4000 – 5000

Figure 4.

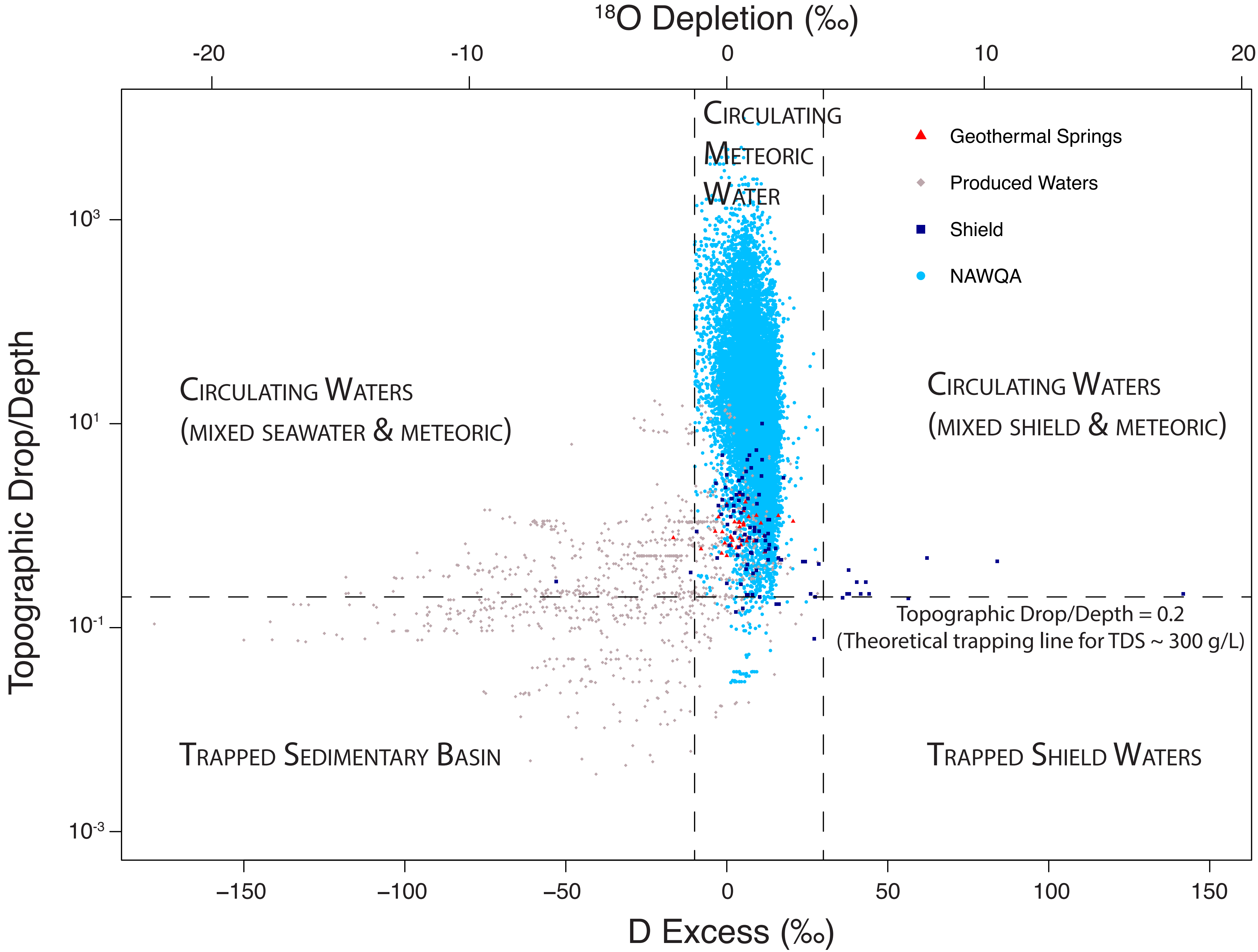

^{18}O Depletion (‰)
-20
-10
0
10
20
Circulating Meteoric Water
Geothermal Springs
Produced Waters
Shield
NAWQA
Circulating Waters (mixed seawater & meteoric)
Circulating Waters (mixed shield & meteoric)
Topographic Drop/Depth
10^{3}
10^{1}
10^{-1}
10^{-3}
Topographic Drop/Depth = 0.2
(Theoretical trapping line for TDS ~ 300 g/L)
Trapped Sedimentary Basin
Trapped Shield Waters
−150
−100
−50
0
50
100
150
D Excess (‰)